



## Electric and magnetic fields and field derivatives from lightning stepped leaders and first return strokes measured at distances from 100 to 1000 m

J. Jerauld,<sup>1,2</sup> M. A. Uman,<sup>1</sup> V. A. Rakov,<sup>1</sup> K. J. Rambo,<sup>1</sup> D. M. Jordan,<sup>1</sup> and G. H. Schnetzer<sup>1</sup>

Received 25 March 2008; revised 4 June 2008; accepted 11 June 2008; published 5 September 2008.

[1] Using electric and magnetic field and field derivative sensors arrayed over an area of about 1 km<sup>2</sup>, we measured the close fields of stepped leaders and first return strokes in 18 negative cloud-to-ground lightning flashes at distances to individual sensors ranging from about 100 m to about 1 km. We present examples of the close field waveforms along with their statistical characterization as a function of the distance to the lightning.

Statistical data are presented for the half-peak width of the stepped-leader/return-stroke electric field waveform; the stepped-leader electric field change; the return-stroke electric field change at 20, 100, and 1000  $\mu\text{s}$  after return-stroke initiation; the peak electric field derivative; the risetime of the electric field derivative waveform; and the magnetic field initial peak, largest peak, risetime, and half-peak width. For example, in the 100–200 m range, the average half-peak width of the leader/return-stroke electric field change was about 0.8 ms; the average observed leader electric field change was about 40 kV m<sup>-1</sup>; the average return-stroke electric field change at 20  $\mu\text{s}$  was about 35 kV m<sup>-1</sup>; and the average peak electric field derivative was about 15 kV m<sup>-1</sup>  $\mu\text{s}^{-1}$ , the largest unsaturated measurement being about 20 kV m<sup>-1</sup>  $\mu\text{s}^{-1}$ . Peak derivative values observed at close range are consistent with derivative measurements made for return strokes over salt water at distances of some tens of kilometers if an inverse-distance dependence is assumed for the field amplitude.

**Citation:** Jerauld, J., M. A. Uman, V. A. Rakov, K. J. Rambo, D. M. Jordan, and G. H. Schnetzer (2008), Electric and magnetic fields and field derivatives from lightning stepped leaders and first return strokes measured at distances from 100 to 1000 m, *J. Geophys. Res.*, 113, D17111, doi:10.1029/2008JD010171.

### 1. Introduction

[2] Negative cloud-to-ground lightning discharges are initiated by downward-moving “stepped leaders” that lower negative charge from the cloud charge source toward Earth at a speed of the order of 10<sup>5</sup> m s<sup>-1</sup>. The stepped leader, whose overall duration is a few tens of milliseconds, is followed by a first “return stroke” that propagates up the leader channel from near ground level to the cloud. The return stroke travels at an initial speed of 1/2 to 1/3 the speed of light and, as it propagates, it drains to Earth the charge previously deposited on the leader channel. Subsequent leader—return-stroke sequences may follow the first sequence, but the subsequent leader is generally a “dart leader”, a leader which moves continuously toward Earth along the main channel of the previous return stroke. A

combined leader—return-stroke process, whether first or subsequent, is referred to as a “stroke”. A general reference to the terminology and the physics of lightning processes is the work of *Rakov and Uman* [2003].

[3] A number of researchers have reported measurements of the characteristics of negative lightning first-return-stroke electric fields and/or field derivatives observed at distances of some tens of kilometers, distances at which the radiation field component of the overall electric field is dominant [e.g., *Weidman and Krider*, 1978; *Cooray and Lundquist*, 1982; *Murray et al.*, 2005]. *Lin et al.* [1979] have measured and characterized negative first-return-stroke electric and magnetic fields at distances from the lightning channel between 1 km and 200 km. Recently, *Jerauld et al.* [2007] described in detail the measured waveshape characteristics of the electric field and the electric field derivative of a negative first-return-stroke observed at the very close distance of about 160 m. They compared those waveshape characteristics with the similar characteristics of a very close, unusual, triggered lightning stroke whose current waveform was recorded. The comparison and modeling were used to argue that the physics behind the initial

<sup>1</sup>Department of Electrical and Computer Engineering, University of Florida, Gainesville, Florida, USA.

<sup>2</sup>Now at Raytheon Missile Systems, Tucson, Arizona, USA.

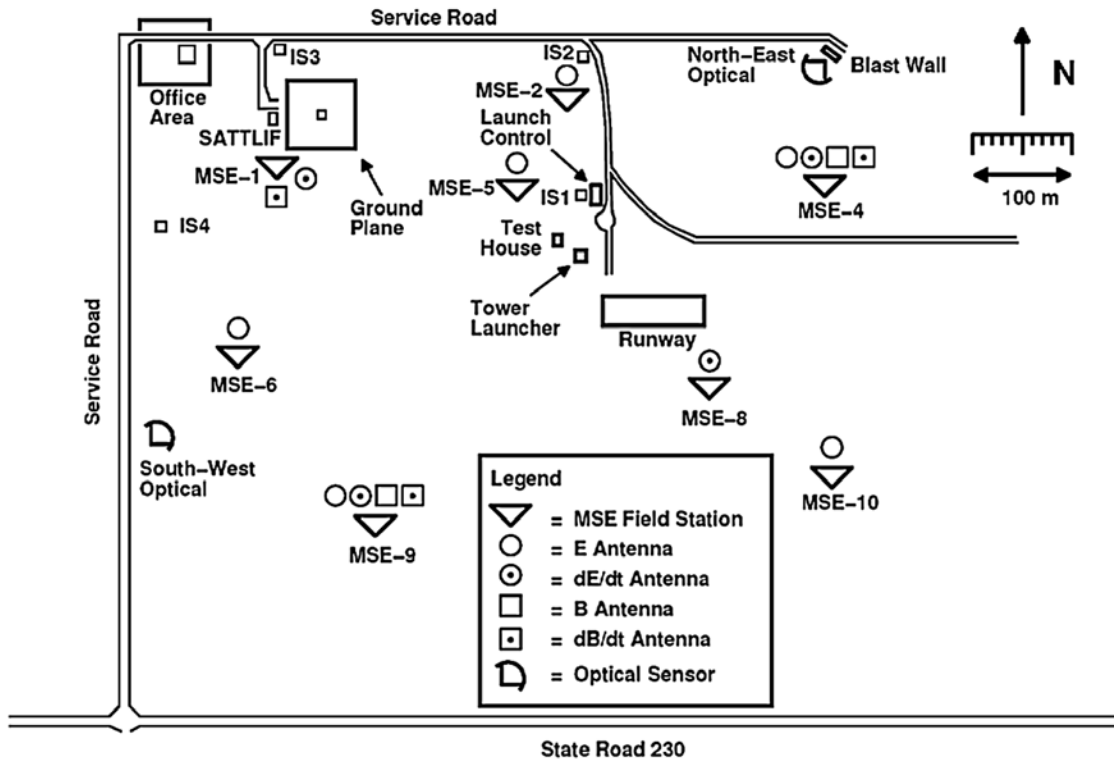


**Figure 1.** Sketch of the MSE system during the 2002–2004 experiments. Objects, except for the MSE field stations and the optical sensors, are approximately to scale.

several-microsecond-duration “slow front” observed (1) in the very close natural and triggered return-stroke electric field waveforms, (2) in the current of the triggered stroke, (3) in typical distant natural lightning first-return-stroke radiation fields, and (4) in typical tower-measured first-return-stroke currents involves a pair of microsecond-duration current waves, each having a peak value of up to some tens of kiloamperes, propagating in opposite directions from the junction point of the descending stepped leader and an upward-moving, connecting leader from the ground.

[4] Electric fields from stepped leaders observed at distances beyond about 1 km have been characterized by a number of investigators [e.g., *Beasley et al.*, 1982; *Rakov and Uman*, 1990]. There have been a few closer measurements [e.g., *Beasley et al.*, 1982], but no systematic study of very close stepped-leader electric fields, that is, field measurements from stepped leaders within 1 km.

[5] In the present paper, we add significantly to the existing data on the fields of very close negative lightning first strokes, presenting examples of and characterizing the measured electric fields of 18 negative stepped leaders and the measured electric fields, magnetic fields, and field derivatives of 18 first return strokes each observed simultaneously at multiple distances ranging from less than 100 m to about 1 km, although every measurement was not successful at every station for every lightning. These data will be useful both (1) in understanding the physics of stepped leaders and first return strokes, and (2) in providing statistical information that can be used to assess the probability of electronic system damage from very close lightning by induced effects. More details regarding the study of very close first strokes reported here, including additional

field waveforms, are found in the Ph.D. dissertation by *Jerauld* [2007].

## 2. Experiment

[6] The data to be presented were acquired in 2002, 2003, and 2004 at the International Center for Lightning Research and Testing (ICLRT), an outdoor facility located on the Camp Blanding Army National Guard Base in north central Florida. The multiple-station field-measuring experiment (MSE) was designed to acquire electric and magnetic field and field derivative waveforms from the five to eight cloud-to-ground lightning flashes expected on average to strike within the roughly 1 km<sup>2</sup> of the MSE network per year. A sketch of the network is shown in Figure 1 and information about the MSE measurements is presented in Table 1 and

**Table 1.** List of MSE Stations and Associated Measurements for the 2002–2004 Experiments

Station <sup>a</sup>	Measurements
1	dE/dt, dB/dt (N-S and E-W components)
2	E field
4	E, B (E-W component), dE/dt, dB/dt, (E-W component)
5	E field
6	E field
8	dE/dt
9	E, B (E-W component), dE/dt, dB/dt (E-W component)
10	E field
NEO <sup>b</sup>	optical signal
SWO <sup>c</sup>	optical signal

<sup>a</sup>Stations 3 and 7 removed prior to the 2002 experiment.

<sup>b</sup>Abbreviations for “north-east optical”.

<sup>c</sup>Abbreviation for “south-west optical”.

**Table 2.** Typical MSE Measurement Configuration Settings for the 2002–2004 Experiment

Sensor	Stations	Amplitude Range <sup>a</sup>	Sampling Rate (MHz)	Record Length	Bandwidth
$E$ field	2, 4, 5, 6, 9, 10	$\pm 65 \text{ kV m}^{-1}$	10	0.4, 0.8, or 1.6 s	$0.2 \text{ Hz}^{\text{b}} - 4 \text{ MHz}^{\text{c}}$
$B$ field	4, 9	$\pm 80 \text{ } \mu\text{T}$	10	0.4, 0.8, or 1.6 s	$10 \text{ Hz}^{\text{d}} - 4 \text{ MHz}^{\text{e}}$
$dE/dt$	1, 4, 8, 9	$\pm 25 \text{ kV m}^{-1} \mu\text{s}^{-1}$	200	4 segments, 5 ms each	$\text{DC} - 20 \text{ MHz}^{\text{e}}$
$dB/dt$	1, 4, 9	$\pm 120 \text{ } \mu\text{T } \mu\text{s}^{-1}$	200	4 segments, 5 ms each	$1.6 \text{ Hz}^{\text{e}} - 20 \text{ MHz}^{\text{e}}$
Optical	NEO, SWO	$-0.1 \text{ to } +0.8 \text{ V}$	10	0.4, 0.8, or 1.6 s	$\text{DC} - 1 \text{ MHz}^{\text{f}}$

<sup>a</sup>Usually limited by the oscilloscope settings, that is, the saturation level of fiber-optic transmitter and other electronics is typically higher.

<sup>b</sup>Limited by the decay time constant of the integrating circuit.

<sup>c</sup>Limited by the digitizer.

<sup>d</sup>Limited by the active integrator.

<sup>e</sup>Limited by the external active filter.

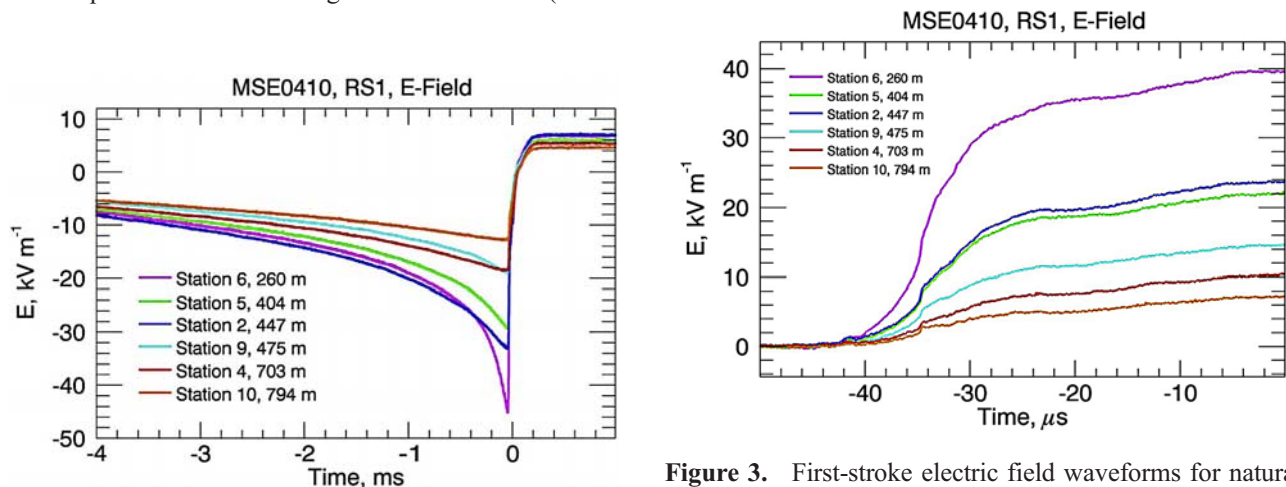
<sup>f</sup>Limited by the preamplifier.

Table 2. The 2002–2004 MSE was composed of six electric field ( $E$ ) measurements, two magnetic field ( $B$ ) measurements, four electric field derivative ( $dE/dt$ ) measurements, four magnetic field derivative ( $dB/dt$ ) measurements, and two optical measurements located at the sites noted in Figure 1 and Table 1. Photographs of the antennas and antenna sites are found in the work of *Jerauld* [2007]. The bandwidths, record lengths, sampling rates, and amplitude ranges of the five types of measurement are given in Table 2. Waveforms from flat-plate antennas ( $E$ ,  $dE/dt$ ) and vertical-loop antennas ( $B$ ,  $dB/dt$ ) were transmitted from the electronics associated with the antennas via Opticom MMV-120C fiber-optic links to the electromagnetically shielded Launch Control Trailer (see Figure 1) where they were low-pass filtered and digitized. The output of a field mill (measuring the cloud quasi-static electric field at ground level) was monitored by a computer which automatically armed/disarmed the MSE when conditions were appropriate/inappropriate for lightning occurrence. The digitizers in the Launch Control Trailer were triggered when the output of the two optical sensors, South-West Optical (SWO) and North-East Optical (NEO) in Figure 1 and Table 1, which viewed the MSE at low altitudes from opposite corners of the network, simultaneously exceeded a threshold, so that data were only obtained for lightning within or very near the MSE network. During 2002, data were acquired from seven negative first strokes (labeled

MSE 0201, 03, 05, 07, 09, 10, 11) and one positive first stroke (MSE 0202); during 2003, from two negative first strokes (MSE 0301,03); and during 2004, from nine negative first strokes (MSE 0401, 02, 03, 04, 07, 09, 10, 11, 12). Data were also recorded for one subsequent (a stroke following the first) positive return stroke and many subsequent negative strokes. In the present paper, we consider only the characteristics of the 18 negative first strokes.

### 3. Measured Waveforms

[7] Figure 2 shows the stepped-leader/return-stroke electric field changes from MSE 0410 at six different stations whose distances from the calculated (see next paragraph) return-stroke strike point ranged from 260 m to 794 m. The leader field change occurs prior to  $t = 0$  in Figure 2. As expected, the largest leader field change (the zero-field level is off the left of the figure) is at the closest station, 260 m from the leader, while the smallest field change is at the most distant station. The fine structure of the return-stroke waveform, which occurs after  $t = 0$ , is not discernable on the 5-ms time scale of Figure 2. The overall leader-return-stroke waveform exhibits the asymmetrical V-shape that is characteristic of close lightning [e.g., *Rubinstein et al.*,



**Figure 2.** First-stroke electric field waveforms for natural flash MSE0410 displayed on a 5-ms time scale. Closer distances are associated with larger field changes.

**Figure 3.** First-stroke electric field waveforms for natural flash MSE0410, displayed on a  $50\text{-}\mu\text{s}$  time scale. Each waveform was vertically shifted so that it would begin with zero amplitude and horizontally shifted so that the fast transition occurs at the same time.

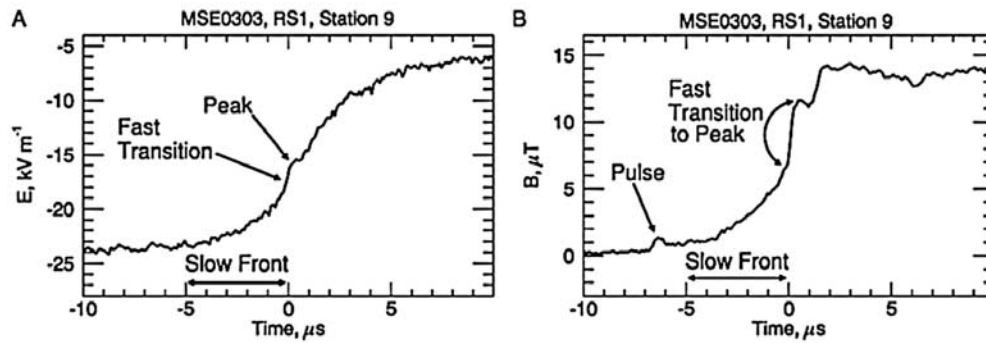


**Figure 4.** First-stroke electric field (A) and magnetic field (B) waveforms for natural flash MSE0303, displayed on a 20- $\mu$ s time scale. The waveforms were both measured at Station 9, which was about 265 m from the channel. Only the east-west component of the azimuthal magnetic field was measured. The waveforms were shifted in time so that the fast transition occurs at time zero.

1995; Crawford *et al.*, 2001], with the transition from leader to return stroke taking place near the bottom of the V.

[8] Clearly, to produce plots such as Figure 2, the distance of the lightning from the measuring stations must be known. Since first-stroke channels are tortuous and

branched, the ground strike point is chosen as the “location of the lightning”. We estimated this location using the “difference of time-of-arrival” method for the peaks of the four  $dE/dt$  signals recorded at stations 1, 4, 8, and 9. Examples of these waveforms are shown later (see Figures 5, 8, and 9).

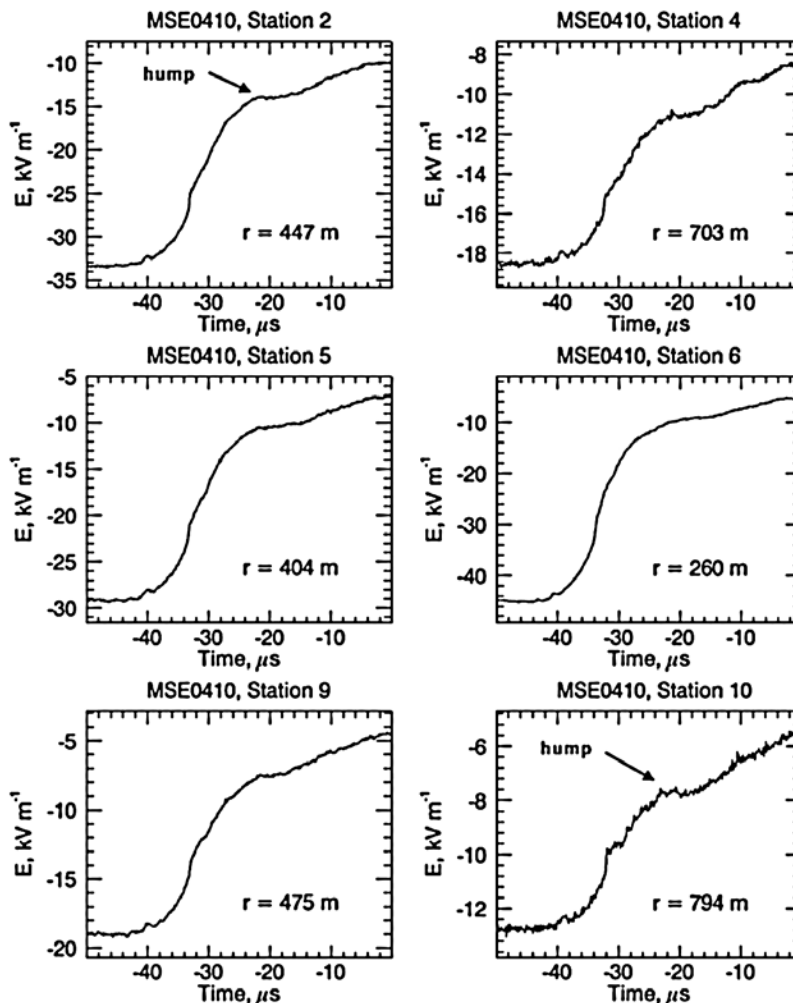


**Figure 5.** Electric field waveforms, measured at six stations, for the first stroke of natural flash MSE0410. Each waveform is displayed on a 50- $\mu$ s time scale.

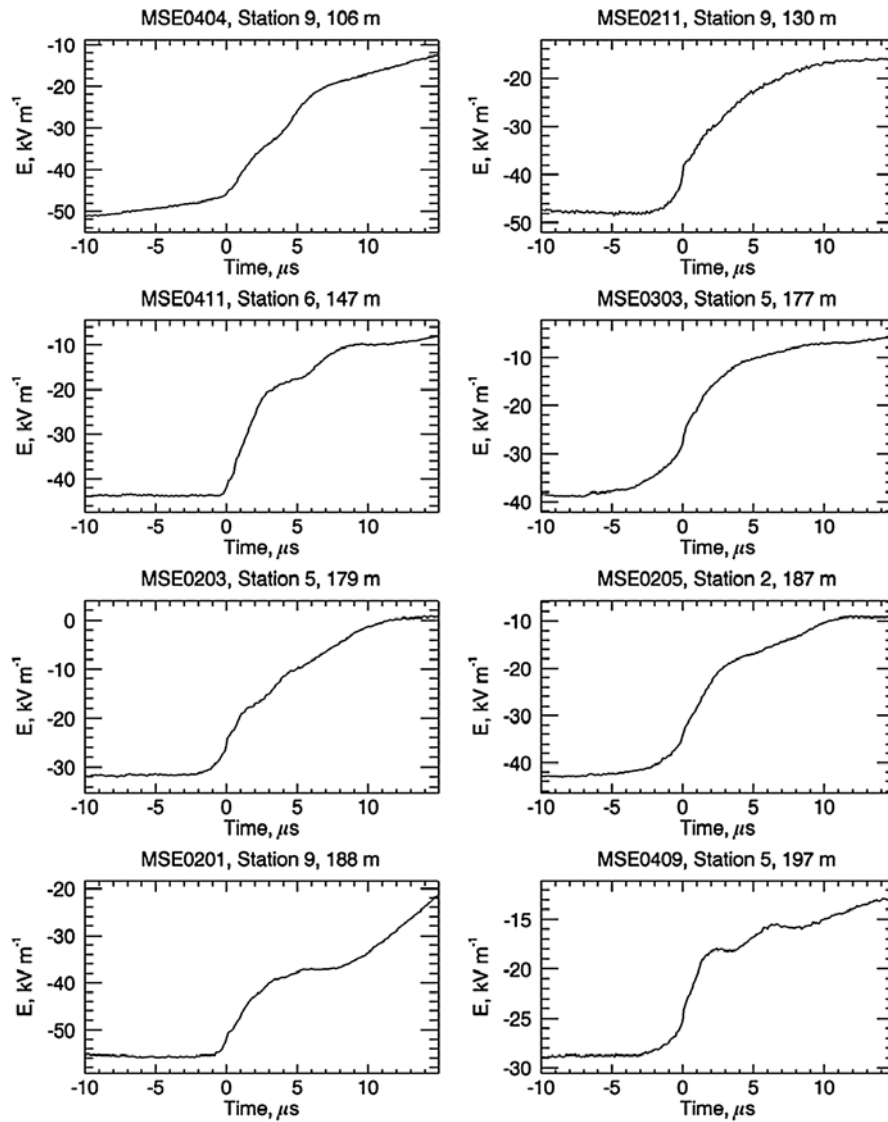


**Figure 6.** Electric field waveforms from eight different first return strokes, all measured between 100 and 200 m of the channel. Each waveform is displayed on a  $25\text{-}\mu\text{s}$  time scale, with time zero corresponding to the fast transition of the waveform.

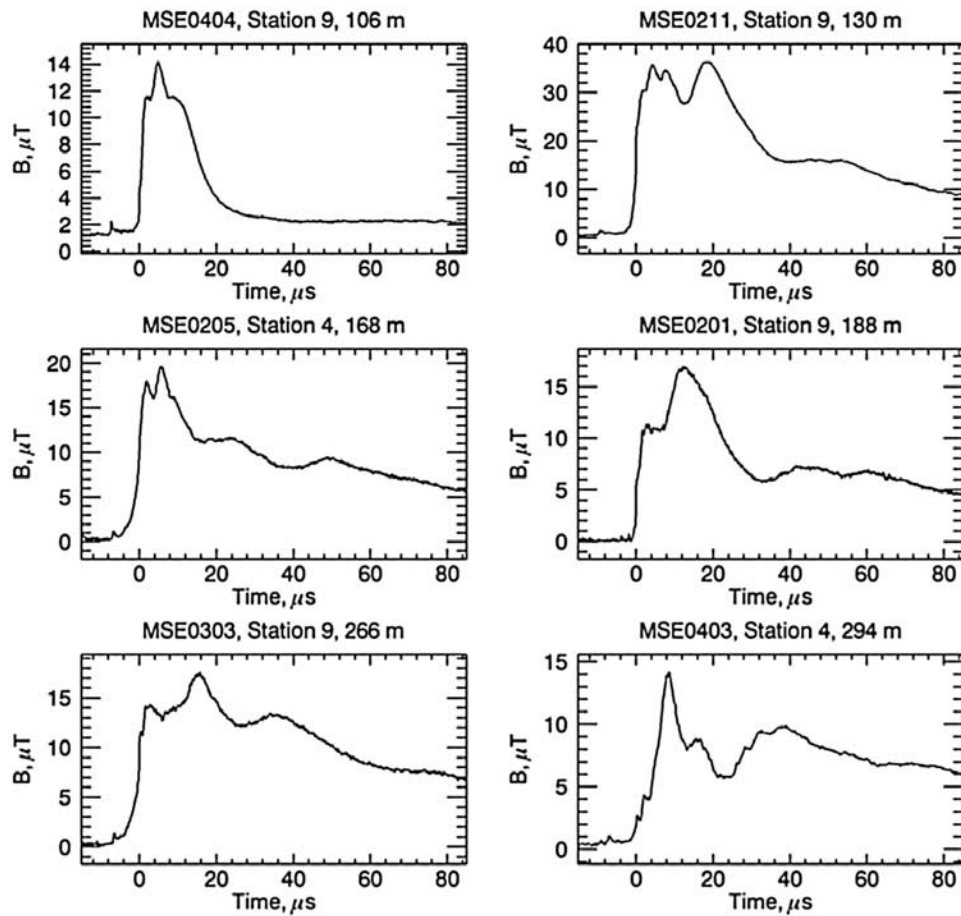


**Figure 7.** Magnetic field waveforms (east-west component only) from six different first return strokes, all measured between 100 and 300 m of the channel. Each waveform is displayed on a 100- $\mu\text{s}$  time scale, with time zero corresponding to the fast transition of the waveform.

If we assume that the source of the  $dE/dt$  peak is located at or very near ground level, two time differences (data from 3 stations) were sufficient to determine a location for lightning striking within the network. The four sets of three-station locations often each produced locations for a given stroke that were within 10 m of each other. For some events, data were available from only three stations, so, while locations could be calculated, the errors could not be

estimated from differences in independent 3-station locations. The largest error in location determined by comparing the locations obtained from sets of three-station location was about 100 m in one direction and about 10 m in the perpendicular direction. When more than one location could be obtained for a given stroke, the locations were averaged. The time-of-arrival locations were complimented by analysis of TV images, a technique that generally exhibited larger

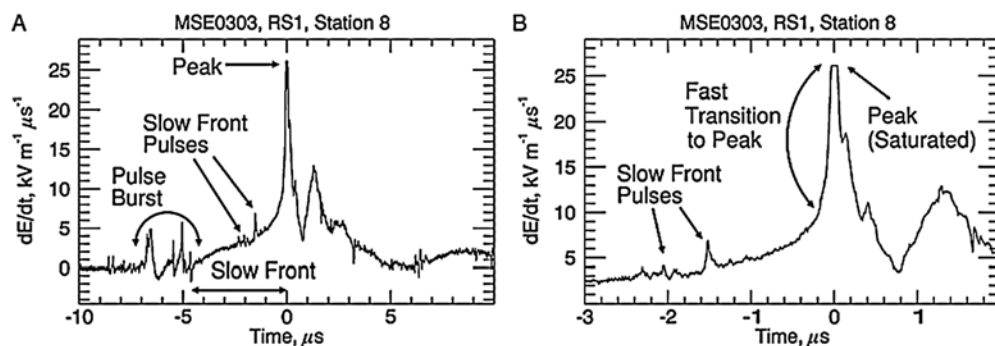


**Figure 8.**  $dE/dt$  waveform from the first stroke of natural flash MSE0303, displayed on a 20- $\mu\text{s}$  (A) and a 5- $\mu\text{s}$  (B) time scale. The waveform was measured at Station 8, which was about 126 m from the channel. The waveform was shifted in time so that the peak occurs at time zero. Features of the waveforms are labeled.

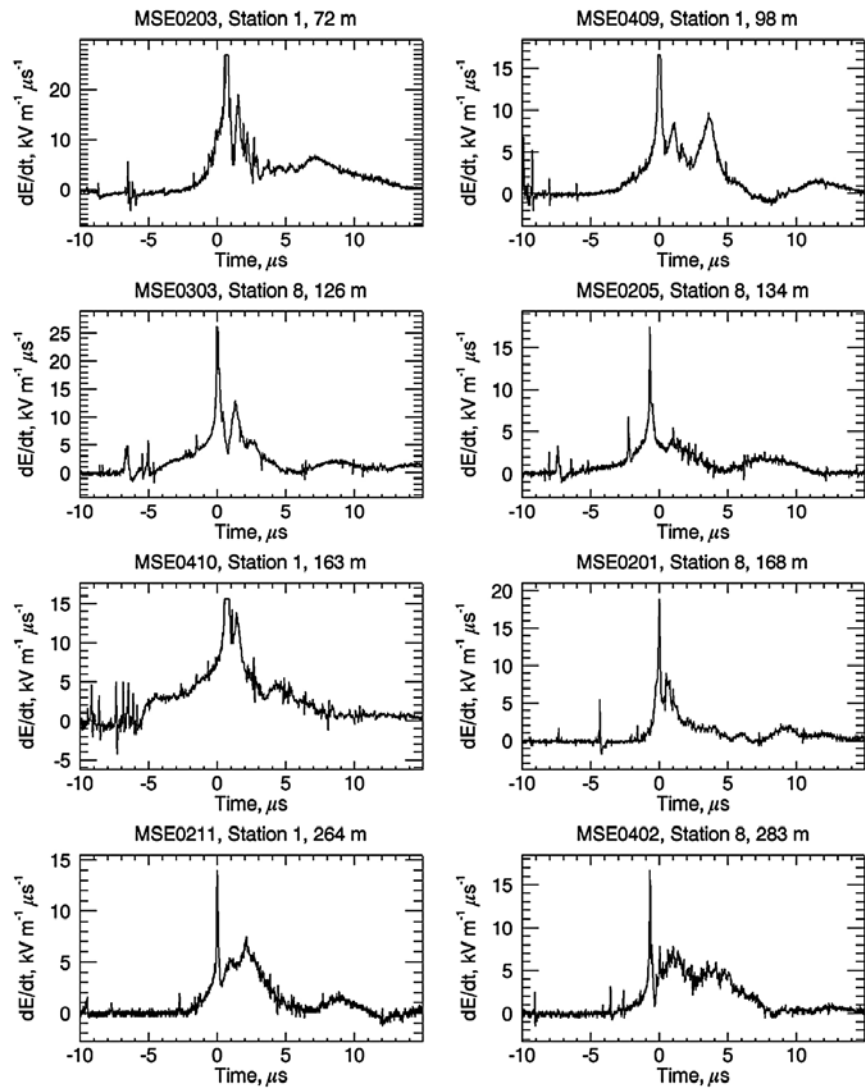


**Figure 9.**  $dE/dt$  waveforms from eight different first return strokes, all measured between 70 and 300 m of the channel. Each waveform is displayed on a 25- $\mu\text{s}$  time scale, with time zero corresponding to the peak of the waveform.

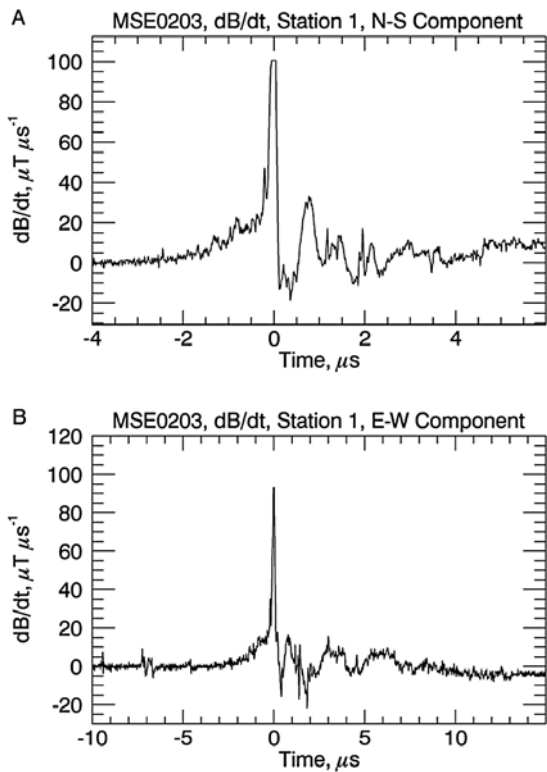


**Figure 10.** North-South (A) and east-west (B) components of  $dB/dt$ , measured at Station 1, at a distance of about 72 m from the first-stroke channel of flash MSE 0203. The north-south waveform is displayed on a 10- $\mu s$  time scale and the east-west waveform on a 25- $\mu s$  time scale, with time zero corresponding to the peak of the waveforms. Note that both waveforms are slightly saturated.

errors than the time of arrival method. Most location errors are thought to be of the order of ten meters, sufficiently small for the present study. The most significant potential error in presented parameters involves the distance between a calculated location and the closest measuring station to that location. In the tables and figures, the distance from a given stroke to the various measurement stations is given to

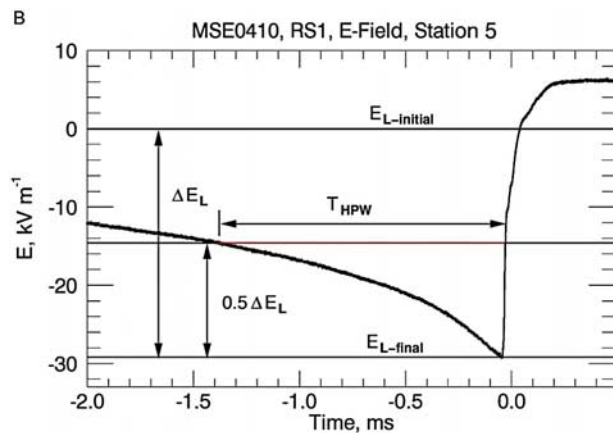


**Figure 11.** First-stroke electric field waveform illustrating the measured leader field change parameters on a 2.5-ms time scale.

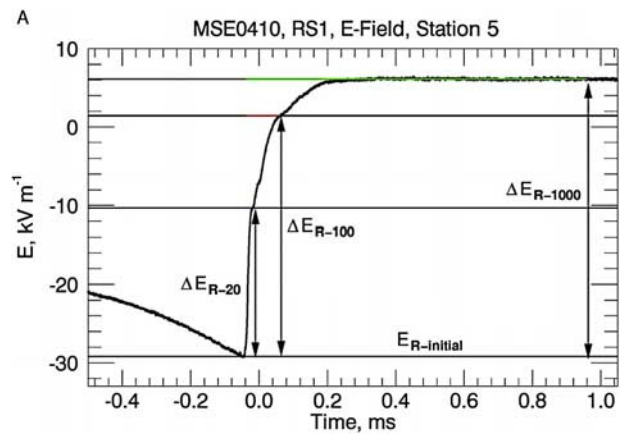


**Figure 12.** First-stroke electric field waveform illustrating the measured return-stroke field change parameters, the field changes from the start of the return stroke to 20, 100, and 1000  $\mu s$ .

three significant figures, as was possible to calculate from a given set of three time differences and the timing accuracy. Clearly, little significance should be attached to the ones-digit.

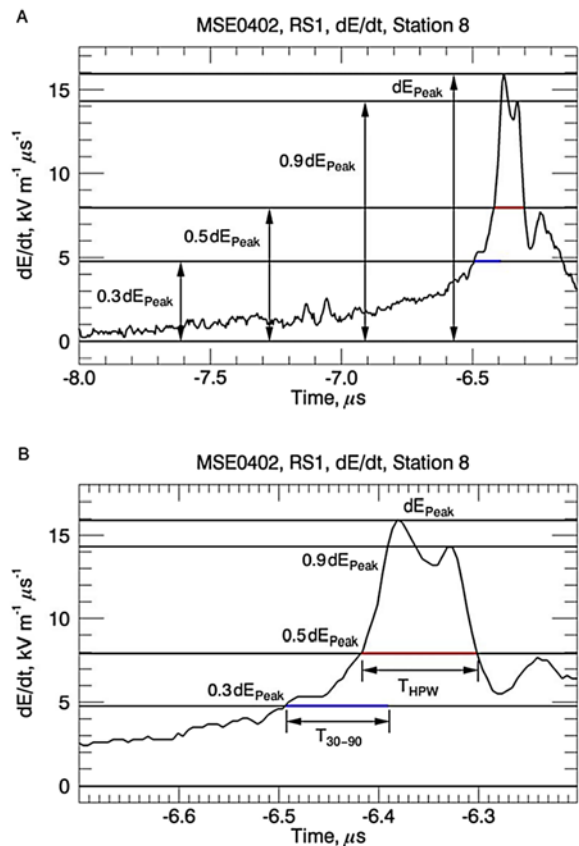


**Figure 13.** First-stroke  $dE/dt$  waveform illustrating the measured waveform parameters. (A) The measured peak value along with the corresponding 30%, 50%, and 90% values. (B) The measured half-peak width ( $T_{HPW}$ ) and the 30%–90% risetime ( $T_{30-90}$ ). “dE” means “ $dE/dt$ ”.

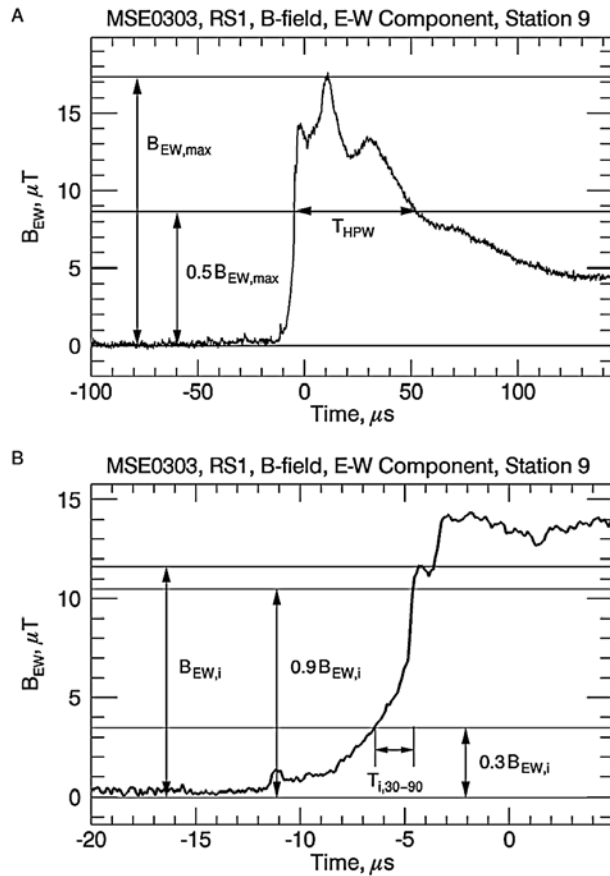


**Figure 14.** First-stroke magnetic field waveform (east-west component only) illustrating the measured waveform parameters. (A) The measured maximum peak value ( $B_{EW,max}$ ) along with the corresponding 50% value and the measured half-peak width ( $T_{HPW}$ ). (B) The measured initial peak value ( $B_{EW,i}$ ) and corresponding 30–90% risetime ( $T_{i,30-90}$ ).

[9] Figure 3 shows an expanded view (to a 50- $\mu\text{s}$  time scale) of the return-stroke portion of Figure 2. The general shape of the return-stroke electric field is an initial “slow front” having a duration of five to ten microseconds, followed by a “fast transition”, which is followed by a slower field change. The slow front and the fast transition to an initial peak (this peak is not always identifiable in very close waveforms) in both electric and magnetic fields are illustrated in Figure 4. This structure has been discussed and modeled by *Jerauld et al.* [2007] and *Jerauld* [2007], as noted in the Introduction. It is clear from Figure 3 that the closer the distance to the lightning, the larger the electric field change. Electric field waveforms on the time scale used in Figure 3 often exhibit “humps” at times ranging from a few microseconds to several tens of microseconds following the fast transition, as is evident from Figure 5 which shows an expanded view of the return-stroke electric field changes at various stations for stroke MSE 0410 of Figure 3. Similar humps are seen in the typical 1 km electric field waveform of *Lin et al.* [1979]. The origin of the humps is uncertain, but charge motion in a channel with major bends and charge motion in major branches (first-stroke

channels commonly exhibit branching) are likely contributors. The slow front and fast transition to peak are more clearly identifiable in Figure 5 at the greater distances, in particular at station 4 at 703 m and at station 10 at 794 m. Figure 6 shows first-return-stroke electric field waveforms from eight different strokes that were observed between 100 and 200 m. They all share the same general characteristics.

[10] Illustrative magnetic field waveforms at distances between 100 and 300 m are presented in Figure 7. These waveforms share similar characteristics, such as an initial peak followed by multiple humps, but there is significant variation between waveforms. An expanded version of the magnetic field of MSE 0303 at a distance of 266 m (lower left of Figure 7) is given in Figure 4B.

[11] Electric field derivative waveforms at a distance of 126 m on two time scales for MSE 0303 are shown in Figure 8. The electric field waveform of MSE 0303 with the slow and fast transition identified is found in Figure 4A. Derivative waveforms from eight different first return strokes in the distance range 70 to 300 m are presented in Figure 9. Derivative waveforms at stations 4 and 9 were integrated so that they could be compared to the directly measured electric fields at those stations. The waveshape match was found to be excellent, but the amplitude of the integrated  $dE/dt$  waveforms was smaller than that of the directly measured electric field, generally by a factor of 1.2 to 2.0, a factor that varied from storm day to storm day. Both electric field and electric field derivative antennas are identical circular flat plates, differing in the circuit elements attached between the plates and ground. The electric field antennas have capacitors, the derivative antennas resistors. Each antenna is surrounded by a ground plane, in part composed of a metal screen. The ground planes, separated by some meters, are attached to separate ground rods and are not bonded together. Photographs are given by *Jerauld* [2007]. All evidence indicates that the electric field antennas are behaving as expected: the various measured field amplitudes decrease with distance as observed in other experiments and as predicted by theory [e.g., *Crawford et al.*, 2001]. This is not always the case for the derivative

**Table 3.** Parameters of the Best Fit Power Law Equations (of the Form  $|\Delta E_L(r)| = Ar^b$ ) for the Measured Leader Electric Field Change Versus Distance for 14 Natural Negative First Strokes<sup>a</sup>

Flash ID	$A$	$b$	$R^2$	Minimum Distance (m)	Maximum Distance (m)
MSE0201	$2.33 \times 10^5$	-1.60	0.72	188	382
MSE0203	$4.53 \times 10^4$	-1.40	0.95	179	587
MSE0205	$5.61 \times 10^4$	-1.40	0.90	166	441
MSE0209	$1.27 \times 10^4$	-1.00	0.86	511	1087
MSE0211	$5.41 \times 10^2$	-0.47	0.71	130	463
MSE0301	$2.52 \times 10^2$	-0.34	0.55	291	872
MSE0303	$1.36 \times 10^3$	-0.68	0.54	177	345
MSE0401	$9.10 \times 10^4$	-1.25	0.91	484	966
MSE0403	$1.04 \times 10^3$	-0.56	0.43	294	899
MSE0404	$9.43 \times 10^2$	-0.69	0.78	106	549
MSE0407	$2.66 \times 10^5$	-1.44	0.79	585	993
MSE0409	$3.98 \times 10^3$	-0.89	0.89	197	615
MSE0410	$1.59 \times 10^4$	-1.05	0.86	260	794
MSE0411	$1.15 \times 10^4$	-1.11	0.93	148	588

<sup>a</sup> $R^2$  = coefficient of determination. Equations obtained for  $\Delta E_L$  in  $\text{kV m}^{-1}$  and  $r$  in meters.

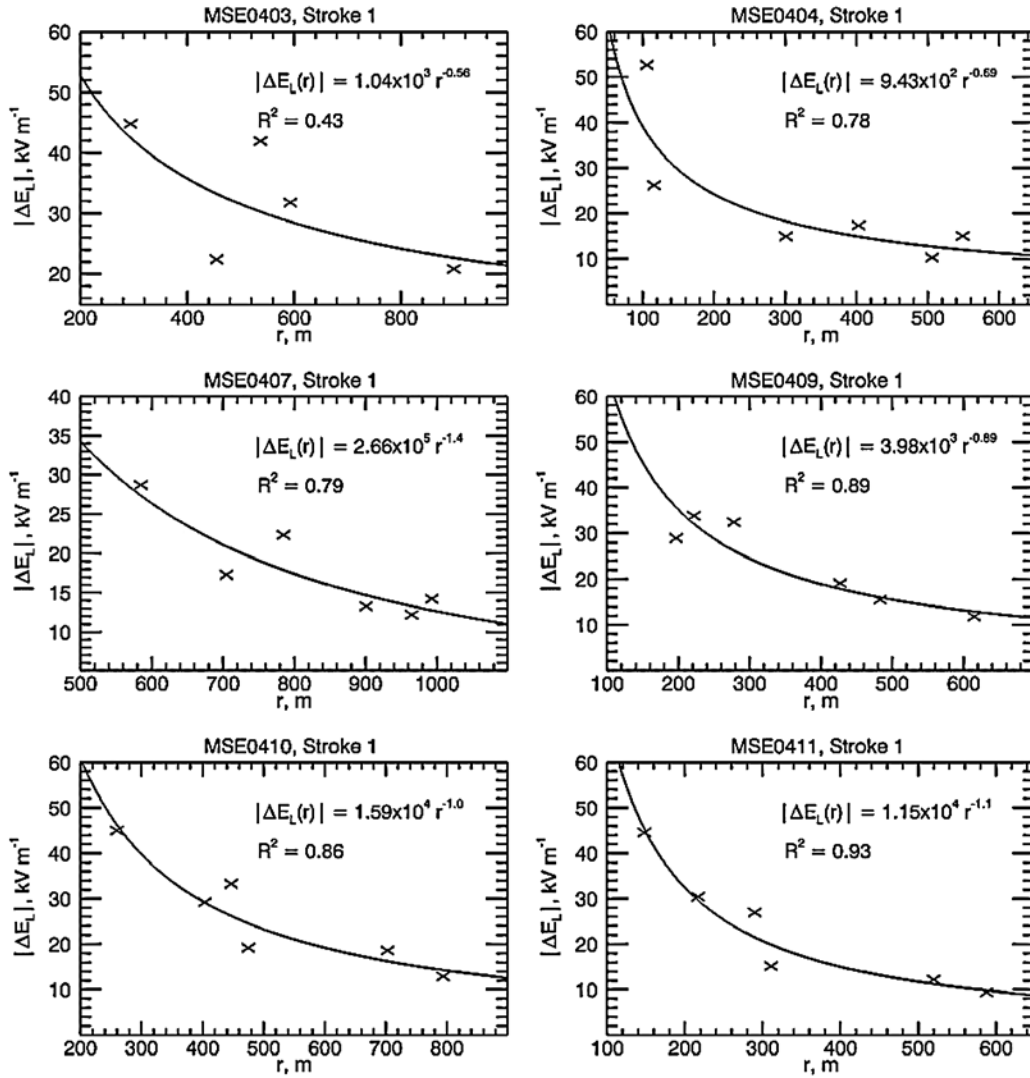


**Figure 15.** Leader electric field change plotted versus distance for the first strokes of flashes MSE0403, MSE0404, MSE0407, MSE0409, MSE0410, and MSE0411. Included on each plot is the best fit power law equation of the form  $|\Delta E_L(r)| = Ar^b$  along with the corresponding coefficient of determination ( $R^2$ ).

antennas, for reasons that remain unclear. In this paper, when derivative amplitudes are presented, they are from stations 4 and 9 and are calibrated to the electric fields measured at those stations by integrating the field derivatives and comparing the integrated field to the directly measured field.

[12] The  $dE/dt$  waveform in Figure 8 exhibits a slow-front/fast-transition combination similar to that seen in the corresponding  $E$  and  $B$  waveforms (Figures 4A and 4B, respectively), but shows much more fine structure. Specifically, multiple pulses are superimposed on the slow front portion of the  $dE/dt$  waveform. Further, a burst of pulses is observed immediately prior to the start of the slow front, which apparently corresponds to a single unipolar pulse observed at the same time in the corresponding  $B$  field waveform. It is unclear if the burst of pulses is in fact the signature of the last downward leader step, or the result of a different process. The close first-stroke  $dE/dt$  waveform presented in Figure 8 is very similar to the distant first-stroke  $dE/dt$  waveforms (which propagated over seawater)

**Table 4.** Parameters of the Best Fit Linear Equations (of the Form  $T_{HPW}(r) = Ar + B$ ) for the Measured Stepped-Leader/First-Return-Stroke Electric Field Half-Peak Width Versus Distance for 14 Natural Negative First Strokes<sup>a</sup>

Flash ID	$A$	$B$	$R^2$	Minimum Distance (m)	Maximum Distance (m)
MSE0201	12.4	-2100	0.87	188	382
MSE0203	3.12	-93	0.88	179	587
MSE0205	10.9	-1300	0.99	166	441
MSE0209	0.741	280	0.96	511	1087
MSE0211	3.14	110	0.83	130	463
MSE0301	0.822	850	0.84	291	872
MSE0303	6.39	-700	0.81	177	345
MSE0401	1.99	-280	0.86	484	966
MSE0403	1.84	300	0.68	294	899
MSE0404	7.61	409	0.82	106	549
MSE0407	1.75	-500	0.82	585	993
MSE0409	7.08	640	0.98	197	615
MSE0410	4.73	-530	0.97	260	794
MSE0411	9.30	-1000	0.95	148	588

<sup>a</sup> $R^2$  = coefficient of determination. Equations obtained for  $T_{HPW}$  in microseconds and  $r$  in meters.

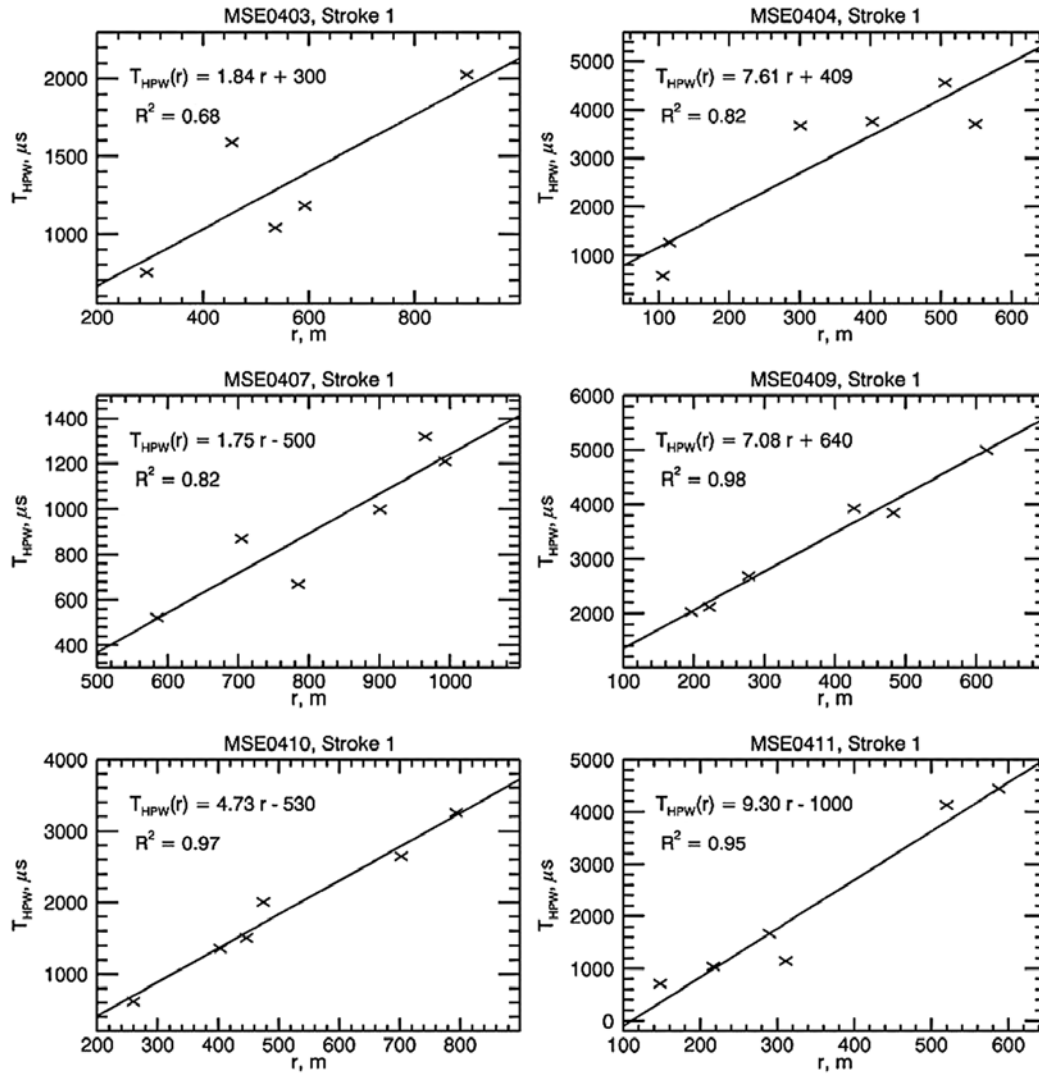


**Figure 16.** Stepped-leader/first-return-stroke electric field half-peak width plotted versus distance for the first strokes of flashes MSE0403, MSE0404, MSE0407, MSE0409, MSE0410, and MSE0411. Included on each plot is the best fit power law equation of the form  $T_{HPWP}(r) = Ar + B$  along with the corresponding coefficient of determination ( $R^2$ ).

**Table 5.** Summary of the Mean Values of  $\Delta E_L$ ,  $\Delta E_R$ , and  $T_{HPWP}$ <sup>a</sup>

Distance (m)	Sample Size	Distance (m)	Mean				$T_{HPWP}$ (ms)
			$\Delta E_L$ (kV m <sup>-1</sup> )	$\Delta E_{R-20}$ (kV m <sup>-1</sup> )	$\Delta E_{R-100}$ (kV m <sup>-1</sup> )	$\Delta E_{R-1000}$ (kV m <sup>-1</sup> )	
100–200	11	160	–41.4	34.4	38.8	39.5	0.767
200–300	16	261	–32.7	25.5	30.8	33.2	1.15
300–400	10	348	–20.2	14.9	19.0	20.7	1.98
400–500	12	449	–22.6	14.5	22.5	23.9	2.19
500–600	11	548	–22.3	16.9	26.5	25.3	2.14
600–700	3	612	–21.9	12.7	18.2	21.5	2.42
700–800	6	743	–20.1	13.0	20.4	24.8	1.74
800–900	4	850	–22.2	7.6	16.4	21.5	1.48
900–1100	8	969	–14.3	11.7	20.2	22.6	1.20

<sup>a</sup>Data sorted by distance into 100-m bins, beginning with 100–200 m, except for the last bin, which contains one value measured at a distance greater than 1000 m.

**Table 6.** Statistics on the First-Return-Stroke Electric Field Change at 20  $\mu\text{s}$ ,  $\Delta E_{R-20}$ <sup>a</sup>

Distance (m)	Sample Size	Mean Distance (m)	$\Delta E_{R-20}$ (kV m <sup>-1</sup> )					
			Mean	Median	Geom. Mean	Standard Deviation	Minimum	Maximum
100–200	11	160	34.4	34.4	33.0	9.4	17.0	46.4
200–300	16	261	25.5	25.1	24.2	8.3	13.1	42.6
300–400	10	348	14.9	13.2	13.7	7.1	6.6	32.1
400–500	12	449	14.5	13.8	12.7	8.0	6.3	33.6
500–600	11	548	16.9	15.4	13.4	12.1	4.7	40.7
600–700	3	612	12.7	9.1	9.7	11.0	4.0	25.0
700–800	6	743	13.0	11.3	11.4	7.2	5.2	24.4
800–900	4	850	7.6	7.0	7.4	2.3	5.8	10.7
900–1100	8	969	11.7	11.9	11.5	2.3	8.4	14.4

<sup>a</sup>Data sorted by distance into 100 m bins, beginning with 100–200 m, except for the last bin, which contains one value measured at a distance greater than 1000 m.

that are presented by Murray *et al.* [2005]. Murray *et al.* observed pulses both immediately prior to and during the slow front, with the slow front pulses appearing similar to the “dominant”  $dE/dt$  pulse (presumably because of the return stroke), which possibly suggests a common or related generation mechanism. Further, Murray *et al.* noted, as we do here, that the exact demarcation between the slow front and the fast transition is not always apparent in the measured waveforms.

[13] In addition to the features described above, the  $dE/dt$  waveforms typically also exhibit one or more secondary pulses, occurring from one to several microseconds after the dominant pulse. These secondary pulses can be a significant fraction of the amplitude of and are longer in duration than the dominant pulse. Also, bursts of small pulses are often observed superimposed on or some microseconds after the secondary pulses. Unlike the stepped leader and slow front pulses (which occur before the dominant pulse), which are always positive, these later-occurring pulses are observed to be both positive and negative.

[14] An example of magnetic field derivative waveforms (two perpendicular components parallel to the ground) at a distance of about 72 m is found in Figure 10. Overall, the  $dB/dt$  waveforms are similar to the  $dE/dt$  waveforms shown in Figures 8 and 9, including features such as the slow front, fast transition, secondary peaks after the dominant peak, and small pulses superimposed on the waveforms both before and after the dominate pulse.

#### 4. Statistical Analysis

[15] Parameters to be measured for a statistical analysis, including the amplitudes, risetimes, and half-peak widths of

the electric and magnetic field and field derivative waveforms, along with additional examples of waveforms, are presented in Figures 11–14.

[16] In Table 3 we present data on the leader field change  $\Delta E_L$  vs. distance  $r$  for 14 individual first strokes. The leader field change is defined in Figure 11. A power law  $Ar^b$  is assumed. A leader field that varies as  $r^{-1}$  ( $b = -1$ ) is indicative of a straight, vertical, uniformly-charged leader channel, at least for the lower kilometer or so of channel [Rubinstein *et al.*, 1995]. Stepped leaders generally exhibit charged branches and are tortuous and non-vertical in the bottom kilometer, and so it is perhaps surprising that an appreciable number of the individual field variations are near the  $r^{-1}$  behavior. Six examples of the data and plots of  $Ar^b$  are presented in Figure 15.

[17] In Table 4 we present the electric field half-peak width  $T_{HPW}$  for the stepped/leader-return-stroke sequence, as defined in Figure 11, for 14 first strokes. A variation  $T_{HPW} = Ar + B$  is assumed. Six examples of the data and the curve fit are found in Figure 16. The half-peak width varies more or less linearly with distance. Table 5 contains the mean value of half-peak width for all available events in 100-m bins. In the 100–200-m bin, the mean of 11 events was 0.77 ms, generally increasing with distance, at least to 700 m or so.

[18] Table 5 also contains the mean values of the leader field change  $\Delta E_L$  (Table 3, Figure 15) in 100-m bins. The overall behavior, as noted earlier, is a decrease in  $\Delta E_L$  with distance. Table 5 further contains the mean values of the three measured return-stroke electric field change parameters, the field change to 20  $\mu\text{s}$ , 100  $\mu\text{s}$ , and 1000  $\mu\text{s}$ , as illustrated in Figure 12. More details on the three return-stroke field change parameters are given in Tables 6–8.

**Table 7.** Statistics on the First-Return-Stroke Electric Field Change at 100  $\mu\text{s}$ ,  $\Delta E_{R-100}$ <sup>a</sup>

Distance (m)	Sample Size	Mean Distance (m)	$\Delta E_{R-100}$ (kV m <sup>-1</sup> )					
			Mean	Median	Geom. Mean	Standard Deviation	Minimum	Maximum
100–200	11	160	38.8	39.5	37.6	9.8	21.6	51.8
200–300	16	261	30.8	29.2	29.4	9.7	17.4	47.9
300–400	10	348	19.0	15.5	17.6	8.4	9.6	38.6
400–500	12	449	22.5	22.6	19.9	11.2	9.4	43.2
500–600	11	548	26.5	30.6	20.9	15.9	6.4	51.0
600–700	3	612	18.2	14.1	14.6	14.4	6.4	34.2
700–800	6	743	20.4	20.9	19.7	5.9	13.5	29.0
800–900	4	850	16.4	16.3	15.6	5.8	11.2	21.7
900–1100	8	969	20.2	18.9	19.9	3.6	16.5	25.2

<sup>a</sup>Data sorted by distance into 100-m bins, beginning with 100–200 m, except for the last bin, which contains one value measured at a distance greater than 1000 m.

**Table 8.** Statistics on the First-Return-Stroke Electric Field Change at 1000  $\mu\text{s}$ ,  $\Delta E_{R-1000}$ <sup>a</sup>

Distance (m)	Sample Size	Mean Distance (m)	$\Delta E_{R-1000}$ ( $\text{kV m}^{-1}$ )					
			Mean	Median	Geom. Mean	Standard Deviation	Minimum	Maximum
100–200	11	160	39.5	41.8	37.9	11.2	21.3	55.5
200–300	16	261	33.2	31.5	31.7	10.2	20.0	51.9
300–400	10	348	20.7	19.4	19.2	8.8	10.6	40.3
400–500	12	449	23.9	24.9	21.2	12.1	10.7	46.0
500–600	11	548	25.3	30.2	19.5	17.0	6.9	54.1
600–700	3	612	21.5	20.6	17.9	14.4	7.6	36.4
700–800	6	743	24.8	24.8	24.4	4.8	17.4	32.1
800–900	4	850	21.5	21.9	21.3	2.4	18.3	23.7
900–1100	8	969	22.6	22.0	22.3	3.7	17.8	28.0

<sup>a</sup>Data sorted by distance into 100-m bins, beginning with 100–200 m, except for the last bin, which contains one value measured at a distance greater than 1000 m.

[19] Statistical data on the peak of the electric field derivative, illustrated in Figure 13, is given in Table 9 for stations 4 and 9 (the two stations which could be calibrated from the co-located electric fields, as discussed earlier). Four  $dE/dt$  measurements were acquired at distances closer than 100 m by stations other than 4 or 9. These measurements were all saturated. Since the integrated derivatives at stations 4 and 9 were always smaller than the co-located directly-measured fields, it is likely that the very close saturated derivative measurements at other stations represent a lower limit to the field derivative within 100 m. The maximum measured  $dE/dt$  value within 100 m was  $28 \text{ kV m}^{-1} \mu\text{s}^{-1}$  and the mean  $24.7 \text{ kV m}^{-1} \mu\text{s}^{-1}$ . Statistics on electric field derivative half-peak width (Figure 13) for all stations are given in Table 10. Statistics on the 30-to-90% risetime of the electric field derivative (Figure 13) are presented in Table 11.

[20] The presence of a finitely conducting ground will influence the measured  $dE/dt$  waveform parameters, including the peak value. Specifically, the peak value observed for the case of propagation over a finitely conducting ground will be lower than the peak that would be observed if the same field propagated over a perfectly conducting ground. The calculations of *Cooray and Ming* [1994] indicate that propagation over 1 km of land having conductivity of  $0.001 \text{ S m}^{-1}$  would decrease the peak field derivative by about 70%. *Rakov et al.* [1998] report a measured value of  $2.5 \times 10^{-4} \text{ S m}^{-1}$  for the soil at the ICLRT, where this experiment was conducted. Despite the fact that propagation

effects likely lowered our measured field derivative peaks from the values that would be observed over perfectly conducting ground, it is of interest to compare the  $dE/dt$  peak values measured here with those obtained for first-stroke waveforms propagating over tens of kilometers of seawater by *Krider et al.* [1996] and *Willett et al.* [1998]. Given the relatively high conductivity of seawater (a few  $\text{S m}^{-1}$ ), the mean value of about  $39 \text{ V m}^{-1} \mu\text{s}^{-1}$  measured by *Krider et al.* and the mean of  $37 \text{ V m}^{-1} \mu\text{s}^{-1}$  measured by *Willett et al.* (all peaks were range-normalized to 100 km assuming a  $r^{-1}$  distance dependence) should be a reasonable representation of first-stroke  $dE/dt$  radiation field peaks in the absence of significant propagation losses. Note that *Willett et al.* claim that there is about a 15% propagation loss for a  $dE/dt$  peak propagating over 22 km of seawater, not reflected in the values given above. Using our mean  $dE/dt$  peak value in the 100–200-m bin,  $14.9 \text{ kV m}^{-1} \mu\text{s}^{-1}$ , and the mean distance of about 150 m, the peak value range-normalized to 100 km is  $22.4 \text{ V m}^{-1} \mu\text{s}^{-1}$ , which is about half the mean value measured by *Krider et al.* and *Willett et al.* However, considering that (1) the sample size of the data presented here is relatively small, (2) some of the  $dE/dt$  waveforms presented here are saturated, (3) the  $dE/dt$  waveform peaks presented here were likely reduced by propagation effects, and (4) the measurement trigger thresholds in these two studies were likely different, there is reasonably good agreement (within a factor of 2) between the mean peak value found here and that given by *Krider et al.* and *Willett et al.*

**Table 9.** Statistics on the First-Return-Stroke  $dE/dt$  Peak, Based Only on Scaled Data Obtained at Stations 4 and 9<sup>a</sup>

Distance (m)	Sample Size	Mean Distance (m)	$dE/dt$ peak ( $\text{kV m}^{-1} \mu\text{s}^{-1}$ )					
			Mean	Median	Geom. Mean	Standard Deviation	Minimum	Maximum
100–200	3	154	14.9	13.9	14.3	5.2	10.2	20.5
200–300	3	284	10.2	10.3	10.1	1.6	8.4	11.7
300–400	5	353	7.1	7.9	6.7	2.3	3.2	9.1
400–500	7	464	7.3	6.8	6.9	2.6	4.2	10.9
500–600	7	552	5.2	4.8	4.3	2.6	0.8	8.6
600–700	ND <sup>b</sup>	ND	ND	ND	ND	ND	ND	ND
700–800	2	736	5.2	5.2	5.1	1.0	4.5	5.9
800–900	2	855	1.8	1.8	1.8	0.1	1.7	1.9
900–1100	4	989	3.1	3.1	3.0	1.0	2.1	4.3

<sup>a</sup>Data sorted by distance into 100-m bins, beginning with 100–200 m, except for the last bin, which contains one value measured at a distance greater than 1000 m.

<sup>b</sup>ND = no data.

**Table 10.** Statistics on the First-Return-Stroke  $dE/dt$  Half-Peak Width,  $T_{\text{HPW}}^a$ 

Distance (m)	Sample Size	Mean Distance (m)	$T_{\text{HPW}}$ ( $\mu\text{s}$ )					
			Mean	Median	Geom. Mean	Standard Deviation	Minimum	Maximum
100–200	5	152	0.145	0.130	0.140	0.041	0.095	0.200
200–300	7	271	0.161	0.153	0.157	0.041	0.116	0.239
300–400	7	358	0.159	0.137	0.152	0.055	0.103	0.250
400–500	16	454	0.174	0.170	0.169	0.044	0.124	0.300
500–600	7	552	0.243	0.244	0.221	0.109	0.118	0.381
600–700	4	662	0.270	0.231	0.255	0.113	0.189	0.430
700–800	5	735	0.279	0.270	0.273	0.072	0.204	0.397
800–900	5	861	0.296	0.299	0.285	0.089	0.187	0.420
900–1100	5	982	0.323	0.361	0.307	0.102	0.170	0.413

<sup>a</sup>Data sorted by distance into 100-m bins, beginning with the 100–200 m, except for the last bin, which contains one value measured at a distance greater than 1000 m.  $T_{\text{HPW}}$  not calculated for waveforms with saturated peaks.

[21] For our measured mean  $dE/dt$  half-peak width, there is a clear trend of increasing with distance. This result is likely due to propagation effects. Return-stroke modeling, assuming propagation over a perfectly conducting ground, predicts a decrease in  $dE/dt$  width with increasing distance. This is the case because at very close distances (within a few hundred meters), the electrostatic component of  $dE/dt$  is significant relative to the radiation component. As distance increases, the contribution of the electrostatic component relative to the radiation component decreases, resulting in a decrease in the width. Also observed is the overall trend of increasing risetime with increasing distance, probably also due to propagation effects, although there is considerable scatter. This scatter is possibly due to the presence of the slow front in the  $dE/dt$  waveforms. The slow front typically has a duration of a 4 or 5  $\mu\text{s}$  and will influence the measured 30-to-90% risetime of  $dE/dt$  if its amplitude is larger than 30% of the peak  $dE/dt$  value. The slow front in  $dE/dt$  is generally more pronounced in closer waveforms, which may explain why the 100–200-m bin has a larger mean 30-to-90% risetime than the following three bins.

[22] Interestingly, for individual first strokes, we often observe little or no discernible dependence of the  $dE/dt$  half-peak width and 30-to-90% risetime on distance. This may be because both of these quantities are simultaneously influenced by (1) propagation effects, (2) the electrostatic component of the field derivative at close distances, and (3) the presence of the slow front in the  $dE/dt$  waveforms. It is not clear how exactly these factors combine to influence the return-stroke  $dE/dt$  waveform parameters.

[23] Statistical data on a variety of first-return-stroke magnetic field parameters, illustrated in Figure 14, are given in Table 12. Note that the bin sizes are chosen differently than in earlier tables. Despite the very small sample size per bin, there is apparently some dependence on distance for each of the waveform parameters, with the exception of the ratio of  $B_i/B_{\text{max}}$ , which appears to be roughly constant at about 0.5. However, only limited conclusions can be drawn from such a small data set, and clearly more data are required in order to compile more meaningful magnetic field statistics. Errors in the location of the lightning will effect the accuracy of the magnetic field amplitude measurements presented since only one magnetic field component was measured. The total field was calculated using the measured azimuth from the loop antenna to the strike location. The ratio  $B_i/B_{\text{max}}$  is unaffected by azimuth error.

## 5. Summary and Conclusions

[24] We have provided a detailed characterization of the electric and magnetic fields of stepped leaders and first return strokes in negative cloud-to-ground lightning at distances from about 100 m to about 1 km. A more complete characterization of the fields of close lightning flashes should include the characteristics of strokes following the first stroke in an overall cloud-to-ground negative discharge. These “subsequent” strokes, as noted in the Introduction, are generally initiated by dart leaders propagating down (and lowering charge on) the defunct first-stroke channel. As a proxy for data on natural subsequent

**Table 11.** Statistics on the First-Return-Stroke  $dE/dt$  30–90% Risetime,  $T_{30-90}^a$ 

Distance (m)	Sample Size	Mean Distance (m)	$T_{30-90}$ ( $\mu\text{s}$ )					
			Mean	Median	Geom. Mean	Standard Deviation	Minimum	Maximum
100–200	5	152	0.244	0.200	0.190	0.187	0.065	0.540
200–300	7	271	0.142	0.160	0.134	0.045	0.061	0.180
300–400	7	358	0.171	0.101	0.131	0.138	0.058	0.370
400–500	16	454	0.229	0.132	0.148	0.287	0.041	1.152
500–600	7	552	0.605	0.403	0.369	0.562	0.055	1.440
600–700	4	662	0.621	0.357	0.318	0.752	0.059	1.710
700–800	5	735	0.415	0.400	0.387	0.150	0.182	0.553
800–900	5	861	0.657	0.328	0.375	0.674	0.100	1.600
900–1100	5	982	0.807	0.400	0.645	0.617	0.372	1.740

<sup>a</sup>Data sorted by distance into 100-m bins, beginning with 100–200 m, except for the last bin, which contains one value measured at a distance greater than 1000 m.  $T_{30-90}$  not calculated for waveforms with saturated peaks.

**Table 12.** Statistics on the Measured Parameters of the First-Return-Stroke Magnetic Field Waveforms Recorded by the MSE System<sup>a</sup>

Distance Range	100–200 m		200–400 m		400–800 m		800–1100 m	
Sample Size	4		8		10		5	
Parameter	Mean	Geom. Mean	Mean	Geom. Mean	Mean	Geom. Mean	Mean	Geom. Mean
Distance, m	144	148	333	330	501	499	946	942
$B_i$ , $\mu\text{T}$	21.1	20.9	15.2	13.3	15.3	12.3	7.6	6.3
$T_{30-90}$ , $\mu\text{s}$	0.5	0.4	1.3	1.2	1.6	1.4	1.5	1.4
$B_{\text{max}}$ , $\mu\text{T}$	37.4	34.2	31.1	24.8	24.7	20.4	14.6	13.6
$T_{\text{HPW}}$ , $\mu\text{s}$	26	25	47	35	78	70	82	69
$B_i/B_{\text{max}}$	0.50	0.48	0.58	0.54	0.58	0.56	0.48	0.46

<sup>a</sup>Data sorted by distance into bins of increasing size, beginning with 100–200 m.

strokes, one may reasonably use equivalent data from strokes in rocket-and-wire triggered lightning flashes since all evidence indicates that these triggered strokes are similar, if not identical, to natural subsequent strokes [Rakov and Uman, 2003]. Schoene et al. [2003] have given wave-shapes and statistical data for the electric and magnetic fields and field derivatives of about 100 triggered lightning return strokes observed at distances of 15 m and 30 m from the stroke channel, while Crawford et al. [2001] have characterized the electric fields of about 20 dart leaders in triggered lightning at distances between 10 m and 621 m, these fields being observed at up to 10 stations simultaneously. Crawford et al. have also compared their results with earlier, less comprehensive dart leader electric field measurements. The combination of the present paper, that of Schoene et al. and that of Crawford et al. provides a relatively complete characterization of the close fields of all negative strokes, both first and subsequent.

[25] **Acknowledgments.** This work was supported in part by U.S. DOT (FAA) grant 99-G-043, NSF grants ATM-0003994 and ATM-0346164, and the Florida Power and Light Corporation.

## References

- Beasley, W. H., M. A. Uman, and P. L. Rustan (1982), Electric fields preceding cloud-to-ground lightning flashes, *J. Geophys. Res.*, *87*, 4883–4902.
- Cooray, V., and S. Lundquist (1982), On the characteristics of some radiation fields from lightning and their possible origin in positive ground flashes, *J. Geophys. Res.*, *87*, 11,203–11,214.
- Cooray, V., and Y. Ming (1994), Propagation effects on the lightning-generated electromagnetic fields for homogeneous and mixed sea-land paths, *J. Geophys. Res.*, *99*, 10,641–10,652. (Correction, *J. Geophys. Res.*, *104*, 12, 227, 1999)
- Crawford, D. E., V. A. Rakov, M. A. Uman, G. H. Schnetzer, K. J. Rambo, M. V. Stapleton, and R. J. Fisher (2001), The close lightning electromagnetic environment: Dart-leader electric field change versus distance, *J. Geophys. Res.*, *106*, 14,909–14,917.
- Jerauld, J. (2007), Properties of natural cloud-to-ground lightning inferred from multiple-station measurements of close electric and magnetic fields and field derivatives, Ph.D. dissertation, University of Florida, Gainesville, Fla. (Available at <http://purl.fcla.edu/fcla/etd/UFE0021279>)
- Jerauld, J., M. A. Uman, V. A. Rakov, K. J. Rambo, and G. H. Schnetzer (2007), Insights into the ground attachment process of natural lightning gained from an unusual triggered lightning stroke, *J. Geophys. Res.*, *112*, D13113, doi:10.1029/2006JD007682.
- Krider, E. P., C. Leteinturier, and J. C. Willett (1996), Submicrosecond fields radiated during the onset of first return strokes in cloud-to-ocean lightning, *J. Geophys. Res.*, *101*, 1589–1597.
- Lin, Y. T., M. A. Uman, J. A. Tiller, R. D. Brantley, W. H. Beasley, E. P. Krider, and C. D. Weidman (1979), Characterization of lightning return stroke electric and magnetic fields from simultaneous two-station measurements, *J. Geophys. Res.*, *84*, 6307–6314.
- Murray, N. D., E. P. Krider, and J. C. Willett (2005), Multiple pulses in  $dE/dt$  and the fine-structure of  $E$  during the onset of first return strokes in cloud-to-ocean lightning, *Atmos. Res.*, *76*, 455–480.
- Rakov, V. A., and M. A. Uman (1990), Waveforms of first and subsequent leaders in negative natural lightning flashes, *J. Geophys. Res.*, *95*, 16,561–16,577.
- Rakov, V. A., and M. A. Uman (2003), *Lightning: Physics and Effects*, Cambridge Univ. Press, New York.
- Rakov, V. A., et al. (1998), New insights into lightning processes gained from triggered-lightning experiments in Florida and Alabama, *J. Geophys. Res.*, *103*, 14,117–14,130.
- Rubinstein, M. F., F. Rachidi, M. Uman, R. Thottappillil, V. Rakov, and C. Nucci (1995), Characterization of vertical electric fields 500 m and 30 m from triggered lightning, *J. Geophys. Res.*, *100*, 8863–8872.
- Schoene, J., M. A. Uman, V. A. Rakov, V. Kodali, K. J. Rambo, and G. H. Schnetzer (2003), Statistical characteristics of the electric and magnetic fields and their time derivatives 15 m and 30 m from triggered lightning, *J. Geophys. Res.*, *108*(D6), 4192, doi:10.1029/2002JD002698.
- Weidman, C. D., and E. P. Krider (1978), The fine structure of lightning return stroke wave forms, *J. Geophys. Res.*, *83*, 6239–6247.
- Willett, J. C., E. P. Krider, and C. Leteinturier (1998), Submicrosecond field variations during the onset of first return strokes in cloud-to-ground lightning, *J. Geophys. Res.*, *103*, 9027–9034.
- J. Jerauld, Raytheon Missile Systems, Tucson, AZ 85714, USA.  
 D. M. Jordan, V. A. Rakov, K. J. Rambo, G. H. Schnetzer, and M. A. Uman, Department of Electrical and Computer Engineering, University of Florida, 311 Larsen Hall, P.O. Box 116200, Gainesville, FL 32611, USA. (uman@ece.ufl.edu)